Water-Soluble Quantum Dots for Multiphoton Fluorescence Imaging in Vivo

Daniel R. Larson, *et al.*

Science **300**, 1434 (2003);
DOI: 10.1126/science.1083780

and morphology of these cells. CagA-mediated recruitment of the scaffolding protein ZO-1 and the tight-junction protein JAM to sites of bacteria attachment on host cell membranes may help to target and retain *H. pylori* at epithelial cell-cell junctions. Localization of signaling molecules, such as SHP2 and Src to CagA in close proximity to the tight junction may alter apical-junctional complex function (*23*, *24*). In addition, we have previously found CagA translocation–dependent changes in gene expression of tight-junction genes in *H. pylori*–infected AGS cells (*25*). One consequence of long-term *H. pylori* infection with CagA+ strains, but not CagA– strains, is a greatly increased likelihood of serious noninfectious sequelae, particularly peptic ulcer disease and gastric cancer. Learning how the long-term disruption of normal apical-junctional complex signaling by CagA could be responsible for these subsequent cellular changes can teach us as much about human biology as it does about the pathogenesis of *H. pylori* infection.

References and Notes

1. R. M. Peek Jr. *et al.*, *Lab. Invest.* **73**, 760 (1995).
2. M. J. Blaser *et al.*, *Cancer Res.* **55**, 2111 (1995).
3. M. Stein, R. Rappuoli, A. Covacci, *Proc. Natl. Acad. Sci. U.S.A.* **97**, 1263 (2000).
4. S. Odenbreit *et al.*, *Science* **287**, 1497 (2000).
5. H. W. Steer, *Gut* **25**, 1203 (1984).
6. S. L. Hazell, A. Lee, L. Brady, W. Hennessy, *J. Infect. Dis.* **153**, 658 (1986).
7. E. Knust, O. Bossinger, *Science* **298**, 1955 (2002).
8. C. Jamora, E. Fuchs, *Nature Cell Biol.* **4**, E101 (2002).
9. D. Bilder, M. Li, N. Perrimon, *Science* **289**, 113 (2000).
10. Materials and methods are available as supporting material on *Science* Online.
11. E. D. Segal, J. Cha, J. Lo, S. Falkow, L. S. Tompkins, *Proc. Natl. Acad. Sci. U.S.A.* **96**, 14559 (1999).
12. W. Fischer *et al.*, *Mol. Microbiol.* **42**, 1337 (2001).
13. S. Censini *et al.*, *Proc. Natl. Acad. Sci. U.S.A.* **93**, 14648 (1996).
14. Single-letter abbreviations for the amino acid residues are as follows: A, Ala; E, Glu; I, Ile; P, Pro; S. Ser; and Y, Tyr.
15. M. Stein *et al.*, *Mol. Microbiol.* **43**, 971 (2002).
16. M. Selbach, S. Moese, C. R. Hauck, T. F. Meyer, S. Backert, *J. Biol. Chem.* **277**, 6775 (2002).
17. H. Higashi *et al.*, *Science* **295**, 683 (2002).
18. H. Mimuro *et al.*, *Mol. Cell* **10**, 745 (2002).
19. E. Papini *et al.*, *J. Clin. Invest.* **102**, 813 (1998).
20. Gentamicin (10μg/ml) in the media for 3 days eliminated viable *H. pylori* from the coculture media, and MDCK cell morphology reverted to normal.
21. C. Yeaman, K. K. Grindstaff, J. R. Wright, W. J. Nelson, *J. Cell Biol.* **155**, 593 (2001).
22. M. R. Amieva *et al.*, unpublished data.
23. C. B. Collares-Buzato, M. A. Jepson, N. L. Simmons, B. H. Hirst, *Eur. J. Cell Biol.* **76**, 85 (1998).
24. V. Nunbhakdi-Craig *et al.*, *J. Cell Biol.* **158**, 967 (2002).
25. K. Guillemin, N. R. Salama, L. S. Tompkins, S. Falkow, *Proc. Natl. Acad. Sci. U.S.A.* **99**, 15136 (2002).

26. Supported by a Pediatric Infections Disease Society of America/St. Jude Fellowship in Pediatric Infectious Diseases (M.R.A.); a Walter V. and Idun Y. Berry Fellowship (R.V.); Deutsche Forschungsgemeinchaft Fellowship VO 864/1-1 (R.V.); and NIH grants DDC DK56339 (R.V., W.J.N., and S.F.), RO1GM35227 (W.J.N.), and AI38459 and CA92229 (S.F. and L.T). We thank T. McDaniels for the use of green fluorescent protein (GFP)–expressing *H. pylori*, F. Bagnioli and M. Goodrich for DNA constructs, S. Censini for the CagA polyclonal antibody, and C. Parkos for the JAM monoclonal antibody.

Supporting Online Material

www.sciencemag.org/cgi/content/full/300/5624/1430/DC1
Materials and Methods
Figs. S1 and S2
Tables S1 and S2
References

26 December 2002; accepted 28 April 2003

Water-Soluble Quantum Dots for Multiphoton Fluorescence Imaging in Vivo

Daniel R. Larson,[1] Warren R. Zipfel,[1] Rebecca M. Williams,[1] Stephen W. Clark,[1] Marcel P. Bruchez,[2] Frank W. Wise,[1] Watt W. Webb[1]*

The use of semiconductor nanocrystals (quantum dots) as fluorescent labels for multiphoton microscopy enables multicolor imaging in demanding biological environments such as living tissue. We characterized water-soluble cadmium selenide–zinc sulfide quantum dots for multiphoton imaging in live animals. These fluorescent probes have two-photon action cross sections as high as 47,000 Goeppert-Mayer units, by far the largest of any label used in multiphoton microscopy. We visualized quantum dots dynamically through the skin of living mice, in capillaries hundreds of micrometers deep. We found no evidence of blinking (fluorescence intermittency) in solution on nanosecond to millisecond time scales.

Quantum dots (QDs) are bright, photostable fluorophores that have a broad excitation spectrum but a narrow Gaussian emission at wavelengths controllable by the size of the material. QDs allow for efficient multicolor imaging of biological samples (*1*) and should be especially useful for fluorescence imaging in living tissues, where signals can be obscured by scattering and competing intrinsic emissions. Multiphoton microscopy enables deep imaging of a variety of biological samples with less overall photobleaching than with wide-field or confocal microscopy, and it has now become the primary fluorescence imaging technique in thick specimens (*2, 3*). For these difficult imaging tasks, we have investigated the two-photon excitation characteristics of QDs and have begun to explore their use for in vivo multiphoton imaging.

For biological applications, robust water-soluble QDs are needed. Several synthesis strategies have been used, such as surface functionalization with water-soluble ligands (*4, 5*), silanization (*6, 7*), and encapsulation within block-copolymer micelles (*8*). Here, we investigated the photophysical properties of water-soluble CdSe-ZnS nanocrystals prepared by a synthesis method based on encapsulation of the nanocrystals within an amphiphilic polymer (*9*).

We measured the two-photon action cross sections of a number of organic and water-soluble QDs of multiple colors. The action cross sections (Fig. 1A) are the product of the nonlinear two-photon absorption cross section σ_{2P} and the fluorescence quantum efficiency (ϕ_f) and provide a direct measure of brightness for imaging (*10*). Our measured values range from ~2000 to 47,000 Goeppert-Mayer units (GM), depending on the particular preparation and excitation wavelength. An action cross section of 47,000 GM is two to three orders of magnitude larger than those of conventional fluorescent probes now in use, and is an order of magnitude larger than those of organic molecules designed specifically for enhanced two-photon absorption (*11*). The measured maximum value of 47,000 GM approaches the theoretical value of 50,000 GM calculated for CdSe QDs (*12*).

We used fluorescence correlation spectroscopy (FCS) (*13*) to measure the number of fluorescent particles in the focal volume from which we calculated the sample concentrations (*14*). The ratio of fluorescent QDs to total QDs is always <1, suggesting in some cases a considerable nonfluorescent fraction (table S1) (*15*).

Two-photon cross sections for the same core sizes with and without the amphiphilic coat (Fig. 1A, green and red) are nearly identical, indicating that passivation of the core-shell nanocrystals within the amphiphilic micelle appears to have little effect on QD brightness. A comparison between the two-photon action

[1]School of Applied and Engineering Physics, Cornell University, Ithaca, NY 14853, USA. [2]Quantum Dot Corporation, Hayward, CA 94545, USA.

*To whom correspondence should be addressed. E-mail: www2@cornell.edu

spectrum of the highest cross section preparation and its single-photon absorption spectrum (with wavelength doubled) shows little correspondence between spectral features, other than an overall decrease with increasing wavelength (fig. S1). Moreover, the action cross sections and FCS results of these water-soluble nanocrystals remained roughly constant over a period of >9 months, and we found no evidence for settling or aggregation of QDs in water over this time period.

The excitation intensity dependence of two-photon FCS is shown in Fig. 1B. The autocorrelation amplitude $G(0)$, which is proportional to the inverse of the number of fluorescent particles in the focal volume, decreases as the excitation power increases. This trend is opposite to triplet transitions or photobleaching effects, which would appear as apparent decreases in concentration [i.e., increases in $G(0)$] with increasing intensity (*16*). The power dependence of the fluorescence remains essentially quadratic (Fig. 1B, inset, red circles), but if the fluorescence counts are normalized by the number of QDs in the observation volume, the fluorescence per QD reaches a limiting value (Fig. 1B, inset, black circles). We show that this observed power dependence is due to saturation of the two-photon excitation probability in the central focal volume along with increased peripheral excitation, resulting in larger effective focal volumes with increasing intensity.

Calculations of the effective two-photon focal volumes for different cross section sizes are shown in Fig. 1C. At cross sections on the order of 200 GM, the volume increase due to saturation effects is less than 10% at powers < 5 to 10 mW (pulse width, 100 fs at 80 MHz) or ~0.06 to 0.1 nJ per pulse. However, at 30,000 GM the effective focal volume begins to increase noticeably at only ~1 mW (~0.01 nJ). This increase in focal volume results in a reduction in optical resolution, leading to "fuzziness" in the images. $1/G(0)$ values (proportional to the effective focal volume V_{eff}) show a power dependence similar to that given by saturation calculations based on a 30,000-GM probe (black circles, Fig. 1C).

FCS correlation functions of organic QDs in hexane and water-soluble QDs taken at nonsaturating intensities (50 to 200 μW) indicate slower translational diffusion than would be expected given the physical site of the nanocrystal (Fig. 1D). As derived from the measured diffusion coefficients, the Stokes-Einstein hydrodynamic radii are 14 nm and 9 nm for the water-soluble and organic QDs, respectively. These hydrodynamic sizes are about 2 to 3 times the dry radii [as determined by transmission electron microscopy (TEM)]. The difference between the dry and hydrodynamic radii suggests strong interactions between the polymeric surface coatings of the nanocrystals and the solvent (*17*).

A previously reported photophysical aspect of QDs has been fluorescence intermittency (blinking) on time scales of 200 μs to hundreds of seconds (*18*). Characterization of blinking and spectral wandering was previously carried out on immobilized nanocrystals (*19*–*21*) where the fluorescence of individual QDs was followed over extended periods of time. However, it is unclear whether the properties of immobilized nanocrystals are the same as those in solution—the more relevant environment for biological studies. Our solution FCS indicates that short-time fluorescence fluctuations are due to molecular diffusion into and out of the focal volume (Fig. 1D), and we find no evidence for temporal fluctuations from other photophysical processes on time scales up to several milliseconds. Cross-correlation FCS, which eliminates detector afterpulsing artifacts, also shows no intermittency on time scales down to ~100 ns (fig. S2). Thus, on these time scales, blinking is sufficiently rare or heterogeneous that no ensemble property emerges.

The measured cross section values we report here are, to our knowledge, the largest two-photon action cross sections reported to date for a fluorescent probe. For a given excitation intensity, the probability of two-photon excitation is as much as three orders of magnitude higher than with conventional probes, and is six orders of magnitude higher than with intrinsic molecules such as NADH (the reduced form of nicotinamide adenine dinucleotide). Because nonlinear excitation of intrinsic components in cells and tissues in multiphoton microscopy can be the primary source of fluorescence background and phototoxicity, increasing the probe excitation probability relative to that of the intrinsic species increases both contrast and sample viability.

To demonstrate the potential of QDs for deep in vivo multiphoton imaging, we imaged mice intravenously injected with

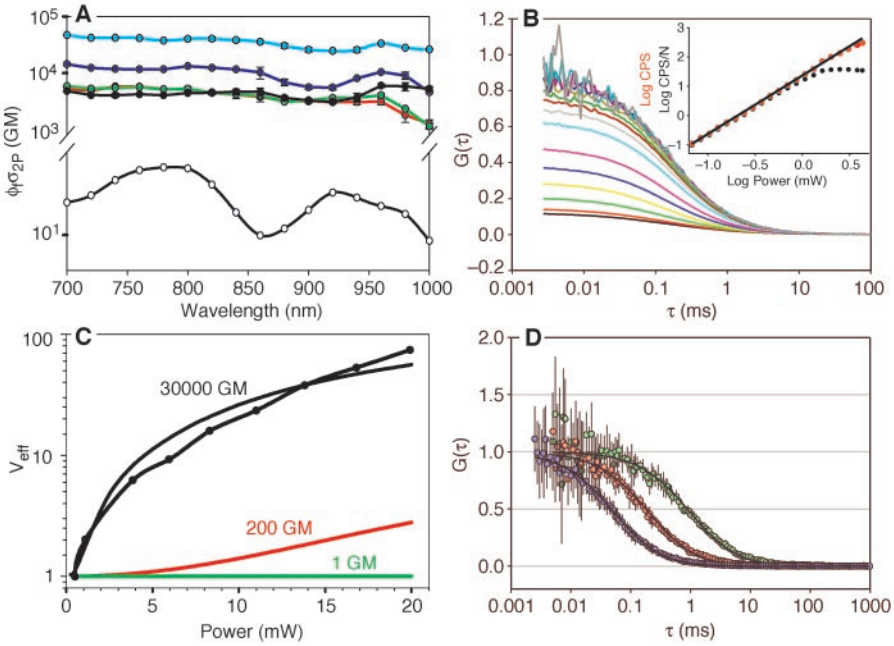

Fig. 1. (**A**) Log plot of two-photon action cross section ($\phi_f\sigma_{2P}$) versus two-photon excitation wavelength for organic QDs, water-soluble QDs of various fluorescence wavelengths, and fluorescein (reference compound). Color code: cyan, 605 nm water-soluble; blue, 567 nm water-soluble; black, 630 nm organic; green, 550 nm water-soluble; red, 550 nm organic; open circles, fluorescein. (**B**) Excitation dependence of the fluorescence correlation function $G(\tau)$ (where τ is the delay) for organic quantum dots. As the intensity increases, $G(0)$ decreases as a result of excitation saturation. Inset: Fluorescence power dependence. The raw count rate (CPS, red) increases as the square of the power while the count rate per molecule (CPS/N, black) saturates. Black line has slope of 2. (**C**) Simulation and experimental results for the effect of excitation saturation of the FCS observation volume. Green, red, and black lines denote calculations for two-photon cross sections of 1, 200, and 30,000 GM, respectively, carried out for 900 nm fluorescence and 1.2 NA (numerical aperture) objective. Black circles, $1/G(0)$ values (proportional to V_{eff}) normalized to $G(0)$ taken at ~100 μW. (**D**) Low-power FCS curves for water-soluble QDs (green circles, excitation power 85 μW at 900 nm) and organic QDs (red circles, excitation power 210 μW at 900 nm). The correlation curves were fit as described in (*14*) and yielded $D_{H_2O} = 1.5 \pm 0.2$ μm²/s and $D_{hexane} = 7.5 \pm 0.6$ μm²/s. A Rhodamine Green correlation curve (blue circles) is shown for comparison.

water-soluble QDs. The size of QDs makes them useful for angiography, analogous to the conventional use of fluorescent dextrans for this purpose (*22*). We examined imaging in the two tissue types we have found to be the most challenging: skin and adipose tissue, both highly scattering tissues with severe refractive index mismatches. Imaging through the intact skin to the base of the dermal layer in a live mouse at 900 nm, we found the QD-containing vasculature to be clearly visible (Fig. 2B). On the basis of the volume and concentration of QDs injected and the blood volume of the mice (~1.6 ml), we estimate the concentration in the blood to be ~1 μM for the experiment shown in Fig. 2, A to C, and ~20 nM in Fig. 2, E and F. At the higher concentration of QDs (1 μM), we were easily able to measure blood flow velocity with the use of line scans (Fig. 2, B and C) [as in (*22*)] and to clearly detect the heart rate from temporal undulations of the capillary wall (Fig. 3C) directly through the skin.

We compared QDs to conventional methods by injecting 70-kD fluorescein isothiocyanate (FITC)–dextran at its solubility limit, corresponding to ~40 μM fluorescein in the bloodstream. An image acquired at the same depth as in Fig. 2A with five times as much power (Fig. 2D) shows considerably less detail, and we were only able to acquire blood flow measurements at roughly half the depth accessible with QDs. This in vivo comparison corroborates the action cross section measurements in Fig. 1: Because the cross sections are higher by three orders of magnitude, use of QDs enables imaging at greater depths than with standard fluorophores, using less average power. The capillary structure in the adipose tissue surrounding a surgically exposed ovary is shown in Fig. 2, E and F. With 780 nm excitation, the autofluorescence from adipose cells clearly appears in optical sections near the surface of the fat pad (Fig. 2E); Fig. 2F shows the projected vasculature through a 250-μm-thick region within this tissue.

Presumably, QDs are cleared from the body before breakdown of the highly protective amphiphilic coat. Although cadmium is known to be toxic, the mice used in these imaging experiments showed no noticeable ill effects after imaging and are being maintained as part of an investigation of long-term QD toxicity—an issue that must be addressed before routine use of cadmium-based QDs for chronic experiments involving valuable transgenic animals can begin.

Quantum dots will become key probes for multicolor fluorescence microscopy and will be especially useful for multiphoton microscopy, where bright probes are needed for the variety of challenging imaging tasks to which multiphoton microscopy is now being applied. We have demonstrated their use as a fluorescence angiography probe, and when conjugated to antibodies or aptamers, they will be bright specific labels useful for tracking cells deep within tissue or for detecting low concentrations of antigens—possibly even directly through the skin, as shown here.

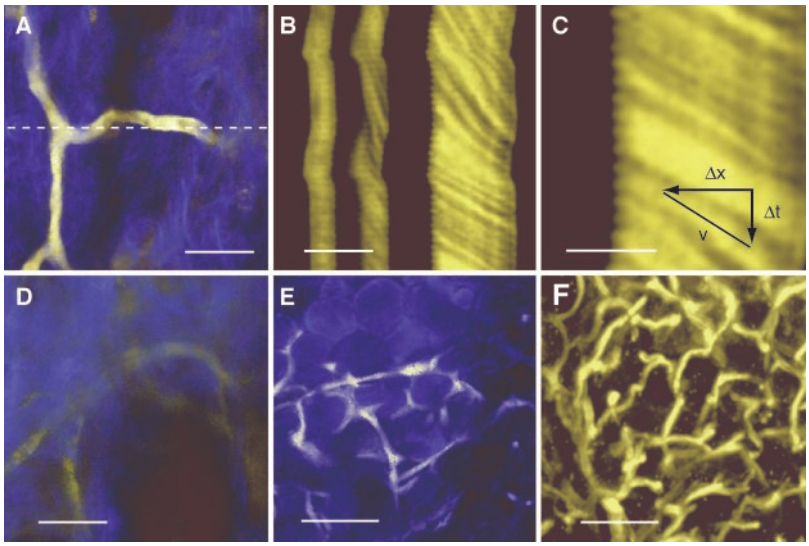

Fig. 2. In vivo imaging of vasculature labeled by a tail vein injection of water-soluble QDs (fluorescence wavelength, 550 nm; TEM diameter, 4.3 nm). (**A**) Fluorescent capillaries containing ~1 μM QDs were clearly visible through the skin at the base of the dermis (~100 μm deep). Excitation at 900 nm was delivered through a 20× 0.95 NA water-immersion objective lens (~40 mW out of the objective, average power at the focal plane unknown); the skin was stabilized by a dorsal skin clamp (fig. S3). Blue pseudocolor is collagen imaged via its second harmonic signal at 450 nm. Dashed line indicates position of line scan shown in (B). (**B**) Line scan (13.7 ms per line) measurement of blood flow velocity taken across capillary in (A). The diameter of this capillary is ~5 μm and the flow is ~10 μm/s. (**C**) Zoom of section in (B) showing undulations in capillary due to heartbeat (640 beats per minute calculated from ripple in the capillary edge; Δx is the spatial dimension of the line scan, Δt is the time dimension, and the hypotenuse is the velocity). (**D**) Comparison image at the same depth as in (A), acquired by injecting FITC-dextran at its solubility limit. (**E**) Image of the surface of adipose tissue surrounding the ovary (blue, autofluorescence; yellow, ~20 nM QDs in blood). Dark circles are adipose cells. (**F**) Projection of capillary structure through 250 μm of adipose tissue (50 images, 5 μm per step). Excitation was at 880 nm for (A) to (C), 780 nm for (D) to (F). Scale bars: 20 μm [(A), (B), and (D)], 10 μm (C), 50 μm [(E) and (F)].

References and Notes

1. W. Chan *et al.*, *Curr. Opin. Biotechnol.* **13**, 40 (2002).
2. W. Denk, J. H. Strickler, W. W. Webb, *Science* **248**, 73 (1990).
3. R. M. Williams, W. R. Zipfel, W. W. Webb, *Curr. Opin. Chem. Biol.* **5**, 603 (2001).
4. W. C. W. Chan, S. Nie, *Science* **281**, 2016 (1998).
5. H. Mattoussi *et al.*, *J. Am. Chem. Soc.* **122**, 12142 (2000).
6. D. Gerion *et al.*, *J. Phys. Chem. B* **105**, 8861 (2001).
7. M. Bruchez, M. Moronne, P. Gin, S. Weiss, P. A. Alivisatos, *Science* **281**, 2013 (1998).
8. B. Dubertret *et al.*, *Science* **298**, 1759 (2002).
9. X. Y. Wu *et al.*, *Nature Biotechnol.* **21**, 41 (2003).
10. C. Xu, W. Zipfel, J. B. Shear, R. M. Williams, W. W. Webb, *Proc. Natl. Acad. Sci. U.S.A.* **93**, 10763 (1996).
11. M. Albota *et al.*, *Science* **281**, 1653 (1998).
12. S. S. Blanton, A. Dehestani, P. C. Lin, P. Guyot-Sionnest, *Chem. Phys. Lett.* **229**, 317 (1994).
13. D. Magde, E. Elson, W. W. Webb, *Phys. Rev. Lett.* **29**, 705 (1972).
14. See supporting data on *Science* Online.
15. Y. Ebenstein, T. Mokari, U. Banin, *Appl. Phys. Lett.* **80**, 4033 (2002).
16. J. Widengren, U. Mets, R. Rigler, *J. Phys. Chem.* **99**, 13368 (1995).
17. In higher viscosity solvents such as hexadecane, the diffusion coefficients scaled as expected. These diffusion coefficients are not altered by sonication, and TEM images reveal predominantly monodispersed particles. These observations allow us to eliminate aggregation as a possible explanation for the measured diffusion coefficients.
18. M. Kuno, D. P. Fromm, H. F. Hamann, A. Gallagher, D. J. Nesbitt, *J. Chem. Phys.* **112**, 3117 (2000).
19. N. Lounis, H. A. Bechtel, D. Gerion, P. Alivisatos, W. E. Moerner, *Chem. Phys. Lett.* **329**, 399 (2000).
20. R. G. Neuhauser, K. T. Shimizu, W. K. Woo, S. A. Empedocles, M. G. Bawendi, *Phys. Rev. Lett.* **85**, 3301 (2000).
21. M. Nirmal *et al.*, *Nature* **383**, 802 (1996).
22. E. J. Yoder, D. Kleinfeld, *Microsc. Res. Technique* **56**, 304 (2002).

23. Supported by NIH grant NCRR P41-RR04224, National Cancer Institute (NCI) grant R33-645644, and NSF grants DBI-0080792 and STC ECS-9876771 (D.R.L., W.R.Z., R.M.W., W.W.W.); Defense Advanced Research Projects Agency grant MDA972-00-1-0021 and NIH grant RR10675 (S.W.C., F.W.W.); and NIH-NCI grant R44CA88391-02 and National Institute of Standards and Technology grant ATP 70NANB0H3000 (M.P.B.). We thank A. Flesken-Nikitin and A. Nikitin for help with the angiography procedure and B. Hyman for its suggested use.

Supporting Online Material

www.sciencemag.org/cgi/content/full/300/5624/1434/DC1
Materials and Methods
Table S1
Figs. S1 to S3
References

24 February 2003; accepted 25 April 2003